JOURNAL OF SOLID STATE CHEMISTRY 35, 215–229 (1980)

Effects of Additions of TiO_2, SnO_2, Ga_2O_3, and MgO on the Phase Equilibria, Stoichiometry, and Lattice Parameter of $Ni_{0.89}Fe_{2.11}O_4$

P. K. GALLAGHER, D. W. JOHNSON, JR., H. SCHREIBER, JR., AND E. M. VOGEL

Bell Laboratories, Murray Hill, New Jersey 07974

Received November 24, 1979; in final form January 30, 1980

Additions up to a mole fraction of 0.1 of TiO_2, SnO_2, Ga_2O_3, and MgO were made to $Ni_{0.89}Fe_{2.11}O_4$. Pellets were equilibrated in O_2, 0.1% O_2 in N_2, and N_2 at 1150, 1250, and 1350°C. Chemical and microstructural analysis enabled the determination of phase boundaries and the mechanisms of charge compensation. Charge compensation for the solubility of the additives in the spinel was predominantly (70%) by Fe^{2+} formation, as opposed to cation vacancy formation, under the more oxidizing conditions and approached 100% under the reducing conditions. Variations in the lattice parameter of the spinel were noted as a function of additive, vacancy, and Fe^{2+} concentrations.

Introduction

Earlier work (*1*) on Ti doped MnZn ferrite clearly demonstrated the ability to determine vacancy concentrations and divalent iron content as a function of firing conditions and Ti content. That information enabled a detailed description of the charge compensation mechanisms associated with the incorporation of Ti^{4+} into the spinel structure. In addition, when the vacancy concentrations were coupled with observations of the phase boundaries, it was possible to correlate the precipitation of a second phase with the attainment of a critical vacancy concentration that was dependent upon the temperature. Whether these vacancies were formed by additions of Ti or from the atmosphere/temperature relationship during firing appeared irrelevant. This was an encouraging start toward a more complete understanding of the solid state chemistry associated with the dissolution of ions in ferrites and the onset of second phase formation. However, there were two difficulties inherent in the earlier work which complicated the detailed interpretation of some of the results. These were the uncertainty in the valence of the manganese (*2*), particularly under the more oxidizing conditions, and the loss of zinc from the ferrite after long heat treatments at high temperatures and low oxygen partial pressures (*3*). Therefore, this expanded sequel to the earlier work uses nickel ferrite in order to eliminate these problems. This has the added advantage of ready access to study not only the hematite phase boundary but also the boundary between spinel and a monoxide phase (*4*) analogous to wustite in the pure iron system.

Additions of TiO_2, SnO_2, equimolar mixtures of TiO_2 and SnO_2, Ga_2O_3, and MgO to iron-rich nickel ferrite, $Ni_{0.89}Fe_{2.11}O_4$, and to a lesser extent iron-deficient nickel ferrite, $Ni_{1.1}Fe_{1.9}O_4$, were studied. The quadrivalent ions, Ti^{4+} and Sn^{4+}, are commonly used additives to ferrite compositions to

0022-4596/80/140215-15$02.00/0

modify the magnetic and electrical properties (*5*). In addition, the trivalent Ga^{3+} and divalent Mg^{2+} ions were selected because they would have some solubility and stability in the spinel structure and a fixed valence to facilitate the interpretation of the results. Charge compensation mechanisms and phase relationships could then be compared for dopant ions of different valence.

Experimental Procedures

Powders were prepared by freeze drying aqueous solutions (*6*). Large quantities of the two master solutions, about 1 *M* with Ni/Fe ratios of 0.89/2.11 and 1.1/1.9, were prepared from nickel and ferrous sulfates. Weighed quantities of aqueous solutions containing the additives were mixed with weighed aliquots of the master solutions prior to freezing. Quantities of solutions were selected to correspond to additions of 0.025, 0.05, and 0.1 moles of cation dopant per mole of initial ferrite. The compounds used as additives were $Ti(CH_3O)_4$, $SnCl_2$, ($Ti(CH_3O)_4$ + $SnCl_2$), $Ga_2(SO_4)_3$, and $MgSO_4$. Powders were also prepared from each master solution without additives.

The freeze dried powders were calcined in flowing N_2 at 900°C for 16 hr. Pellets of calcined powder were prepared by pressing without binders or lubricants at 31 MPa (4500 psi) in a 1-cm-diameter die. These pellets were then fired at 1150, 1250, or 1350°C for 16 hr in flowing N_2, 0.1% O_2 in N_2, or O_2 and quenched into water. The advantage of quenching in water was established earlier (*1*).

Coulometric titrations (*7*) were performed in triplicate to determine the divalent iron content for each composition and firing. A portion of each sample was polished and examined by optical microscopy for the presence of second phase. Those samples which were suspected of having a second phase were also examined by X-ray diffraction for verification. Quantitative analysis of the various phases was performed with an ETEC electron microprobe. X-Ray intensity ratios of the cations compared to pure metallic standards were analyzed using MAGIC (*8*) for data reduction. Oxygen was determined by difference. An exitation voltage of 20 keV and counting times of 10 sec were used. Several areas were sampled for each phase and the results averaged.

Detailed X-ray diffraction studies were performed on selected samples within the single phase spinel region in order to determine the change of lattice parameter with vacancy content and dopant concentration. A Diano XRD-8000 Diffractometer with 3° and 0.2° slits on the source and counter side, respectively, was used in conjunction with a medium resolution Soller slit and a graphite single crystal monochromater. The goniometer was automatically stepped in 0.01° increments of 2θ while counting for 40 sec at each point. The radiation used with Cu$K\alpha_1$.

The samples were ground and mixed with the high-purity silicon used as an internal standard. A single sample, $Ni_{0.89}Fe_{2.11}O_4$ + 0.1 TiO_2 fired at 1150°C in N_2, was initially used to establish the best technique and peaks for use in determining the lattice parameter. The 620 and 533 Si peaks (2θ = 127.53386 and 136.87990) were used to correct the 844 and 951 peaks of the spinel, respectively. A series of five measurements were made where the sample was removed and repositioned each time. Peak positions were initially determined by two methods. Method II used the 10 consecutive points of maximum intensity to fit a parabola by least-squares techniques. The 2θ and intensity values at the maximum were then evaluated by setting the first derivative equal to zero. In Method I the background intensity was then subtracted from the peak intensity derived by method II and a level of 2/3 maximum intensity was established. This is generally very near the

point of inflection on the sides of the peak. The 10 consecutive points centered on this intensity were fit to a straight line by least-squares techniques for both sides of the peak and the exact 2θ values corresponding to 2/3 maximum intensity were calculated. The values of 2θ at this intensity for both sides of the peak were averaged to give the peak position based upon the assumption of a symmetrical peak.

Table I lists the differences between the observed and theoretical values of 2θ for the Si peaks that were used to correct the observed values of 2θ for the spinel. The corrections are large and variable ranging from $+0.03$ to $-0.06°$. The variation in magnitude is smaller using the higher angle spinel peak, 951, and Method I shows somewhat less variation than Method II. Corrected values of the lattice parameter, a, are given in Table II. It is immediately obvious that the corrections are vital since, in the best case, a spread of 1 part in 85,000 is achieved in the corrected value while the individual corrections predict changes in a of 1 part in 16,000. The second obvious conclusion is that Method I combined with the higher angle peak represents the more precise technique for evaluating the lattice parameter and further values reported herein are based upon this method of analysis.

TABLE I

CORRECTIONS TO 2θ USING Si FOR $Ni_{0.89}Fe_{2.11}O_4$ + 0.1 TiO_2 1150°C/N_2

Measurement number	Method I		←hkl→	Method II	
	844	951		844	951
1	+0.0313	−0.0095		+0.0275	−0.0171
2	+0.0012	−0.0313		−0.0009	−0.0352
3	−0.0149	−0.0036		−0.0160	−0.0056
4	+0.0026	−0.0510		+0.0047	−0.0569
5	−0.0535	−0.0435		−0.0603	−0.0547
Mean	−0.0067	−0.0278		−0.0090	−0.0339
SD	±0.0310	±0.0207		±0.0327	±0.0226

Results and Discussion

Fe^{2+} Concentrations

The appendix gives the average values for Fe^{2+} determined for the fired samples.

Phase Relationships

A summary of the phase relationships is presented in Fig. 1. The lines are only approximate since the experimental grid is rather coarse (3 temperatures by 4 concentrations). Nevertheless the trends are clearly demonstrated. Each curve represents the phase boundary associated with a particular additive.

In pure oxygen at ~1100°C there exists only single phase spinel for the undoped material or for any dopings of Mg^{2+} or Ga^{3+}

TABLE II

LATTICE PARAMETER FOR $Ni_{0.89}Fe_{2.11}O_4$ + TiO_2 1150°C/N_2[a]

Measurement number	Method I		←hkl→	Method II	
	844	951		844	951
1	0.835321	0.835319		0.835331	0.835343
2	0.835277	0.835318		0.835284	0.835326
3	0.835203	0.835314		0.835204	0.835316
4	0.835256	0.835309		0.835393	0.835309
5	0.835183	0.835309		0.835393	0.835309
Mean	0.835248	0.835319		0.835290	0.835328
SD	±0.000057	±0.000011		±0.000075	±0.000016

[a] Values in nanometers.

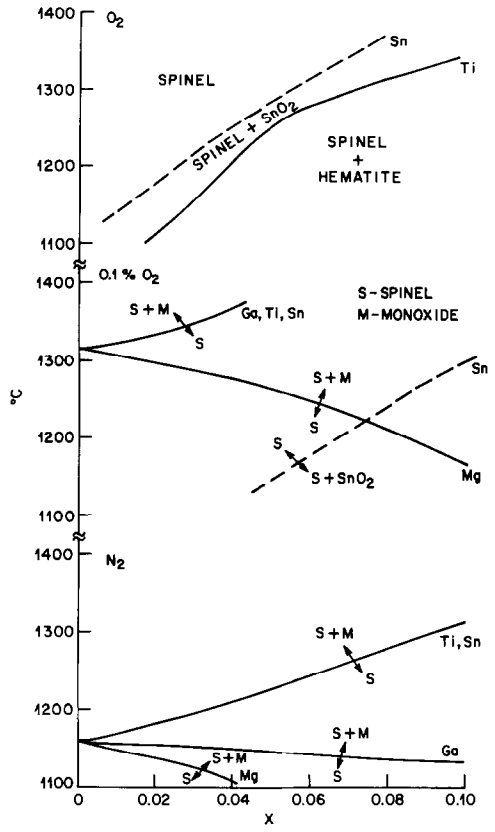

FIG. 1. Phase boundaries of $Ni_{0.89}Fe_{2.11}O_4 + xMO_y$ in various atmospheres. S = Spinel; M = monoxide.

within the range investigated. Solubility of SnO_2 (dashed curve) is limited and increases with increasing temperature as expected. Substitution of Ti^{4+} leads to hematite precipitation (solid curve) which increases with increasing concentration or decreasing temperature.

In 0.1% O_2 hematite precipitation does not occur in the region studied. The solubility of SnO_2 has increased markedly but at lower temperatures it is exceeded (dashed curve). In this less oxidizing atmosphere the monoxide, (NiFe)O, phase becomes a factor. Substitution of the fixed divalent Mg^{2+} ion particularly enhances the precipitation of the monoxide phase. The effects of trivalent or quadrivalent substitutions will tend to suppress this precipitation. These conclusions are based upon the slopes of the boundaries in Fig. 1 and are in accordance with intuitive expectations. Substitution of ions of lower valence than the average in the stoichiometric spinel (2.67) will encourage precipitation of the divalent phase while those of higher valence will encourage precipitation of the trivalent phase.

In N_2 (ppm $O_2 \leq \sim 2$) the monoxide phase becomes more dominant. The trivalent additive, Ga, has little effect upon the position of the phase boundary. The divalent and quadrivalent additives show the same tendencies as before but shifted markedly in favor of the monoxide.

The starting materials that were Ni rich, i.e., $Ni_{1.1}Fe_{2.9}O_4$, always had a monoxide present except for the single exception of the highest concentration of the quadrivalent substitutions fired in O_2. This highest concentration of a 4^+ ion, 0.1 moles, nearly returns the charge balance to stoichiometry in the absence of other effects by compensating for the 0.1 mole of excess divalent Ni. This compensation, however, was only adequate to prevent monoxide formation in the most oxidizing atmosphere.

Distribution of the additives among the phases was determined by microprobe measurements on selected samples. Changes in the Fe/Ni ratio were also determined. Results are presented in Figs. 2–4 and Tables III–V. Type I material will be defined as single phase and the analytical results of two such samples are given in Table III. Agreement with that predicted based upon the preparation data (Fe/Ni = 2.33) is excellent. The Fe/Ni ratio 2.33–2.34 is indicative of the single phase spinel region.

Type II material is defined as two-phase material containing an oxidized phase of SnO_2, a hematite like phase (Fig. 2), or both (Fig. 3). Examples are given in Table IV. In these cases the hematite-like precipi-

TABLE III

MICROPROBE ANALYSIS: TYPE I MATERIALS—SINGLE-PHASE SPINEL

Firing	Dopant	Composition	Fe/Ni
1150°C/O_2	0.1 Ga	$Ni_{0.898}Fe_{2.102}Ga_{0.100}O_{4+\beta}$	2.34
1250°C/0.1%	0.05 Ti	$Ni_{0.900}Fe_{2.100}Ti_{0.032}O_{4+\beta}$	2.33

tate is very rich in iron and the Fe/Ni ratio in the spinel phase is significantly reduced. In addition, the higher valent additives are concentrated in the precipitate as would be predicted. The SnO_2 phase is present as very small particles evident in Fig. 3.

Type III materials are those exhibiting monoxide precipitation (see Fig. 4). As revealed in Table V, this monoxide phase is high in Ni as would be expected. Consequently, the Fe/Ni ratio in the spinel is raised beyond the single-phase value depending upon the amount and composition of monoxide phase that has precipitated. The divalent additive Mg prefers the monoxide phase while the higher valent additives prefer to remain in the spinel. The iron content in the monoxide phase is decreased by the incorporation of small amounts of additives into the monoxide.

Oxygen Stoichiometry and Charge Compensation in the Spinel Phase

Dissolution of the various ions into nickel ferrite requires some form of charge compensation. Coupled with this effect is that induced by the firing temperature and P_{O_2}. In principle this combined charge compensation could be accomplished solely by adjusting the uncharged cation vacancy content (Eq. (1)) or the Fe^{2+}/Fe^{3+} ratio (Eq. (2)) but in reality is achieved by a combination of these two modes (Eq. (3)).

$$(NiFe)^2 + Fe_2^{3+}O_4 + xMO_Y \rightarrow (NiFe)^{2+}Fe_2^{3+}M_x^{2y+}V_\alpha O_{4+xy} \quad (1)$$

$$TiO_2 \rightarrow Ti_{sp}^{4+} + 2\,O_{sp}^{2-} + 1/2\,V_{sp} \quad (1a)$$

$$1/2\,Ga_2O_3 \rightarrow Ga_{sp}^{3+} + 3/2\,O_{sp}^{2-} + 1/8\,V_{sp} \quad (1b)$$

$$MgO \rightarrow Mg_{sp}^{2+} + O_{sp}^{2-} - 1/4\,V_{sp} \quad (1c)$$

$$(NiFe)^{2+}Fe_2^{3+}O_4 + xMO_Y \rightarrow (NiFe)^{2+}Fe_k^{2+}Fe_{2-k}^{3+}M_x^{2y+}O_{4+4/3x} + \frac{(y - 4/3)x_{O_2}}{2} \quad (2)$$

$$TiO_2 + 4/3Fe_{sp}^{4+} \rightarrow Ti_{sp}^{4+} + 4/3Fe_{sp}^{2+} + 4/3\,O_{sp}^{2-} + 1/3\,O_2 \quad (2a)$$

$$1/2\,Ga_2O_3 + 1/3Fe_{sp}^{3+} \rightarrow Ga_{sp}^{3+} + 1/3Fe_{sp}^{2+} + 4/3\,O_{sp}^{2-} + 1/12\,O_2 \quad (2b)$$

$$MgO + 2/3Fe_{sp}^{2+} \rightarrow Mg_{sp}^{2+} + 2/3Fe_{sp}^{3+} + 4/3\,O_{sp}^{2-} - 1/6\,O_2 \quad (2c)$$

$$(NiFe)^{2+}Fe_2^{3+}O_4 + xMO_Y \rightarrow (NiFe)^{2+}Fe_k^{2+}Fe_{2-k}^{3+}M_x^{2y+}V_\alpha O_{4+\beta} + nO_2 \quad (3)$$

Symbols used in the earlier work (*1*) are preserved. M represents the cation additive, x is the number of moles of additive incorporated into the spinel (sp), k is the change in divalent iron content from the initial stoichiometric ferrite, and α is the vacancy concentration per formula unit. Table VI gives the rate of change of α and k with x for the limiting cases of Eqs. (1) and (2).

The variables in Eqs. (1)–(3) are not independent and the following relationships can be readily derived.

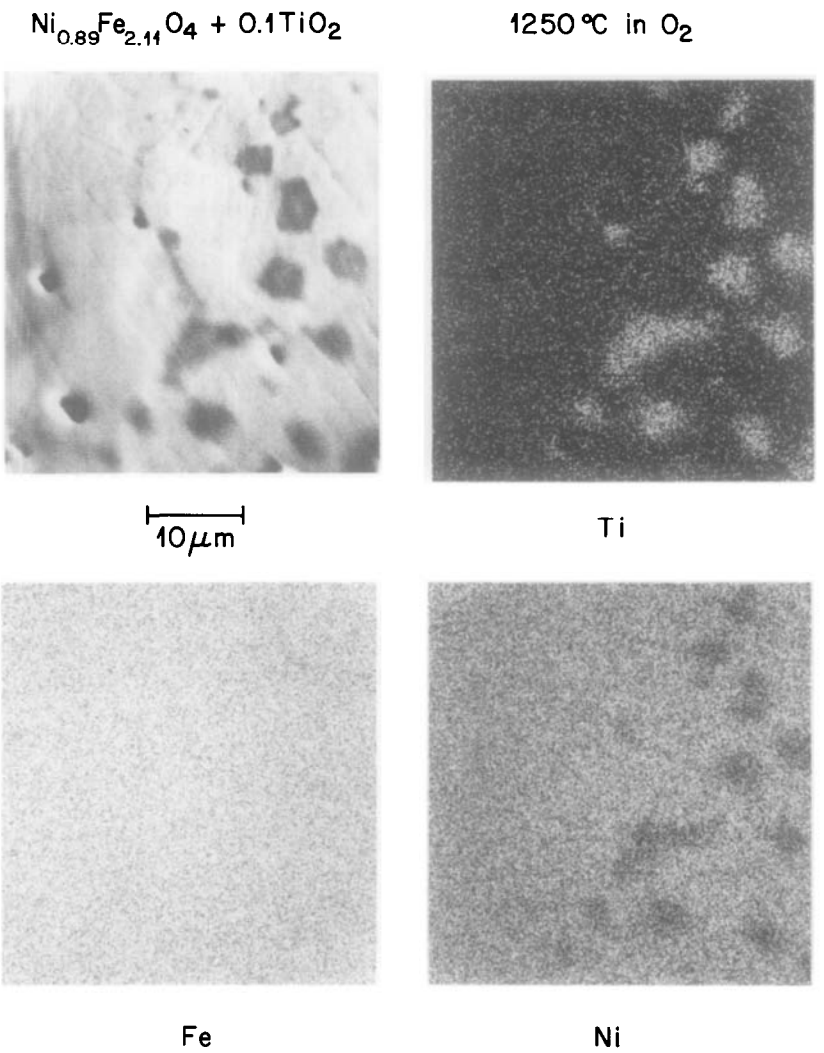

FIG. 2. Electron and elemental characteristic X-ray images of $Ni_{0.89}Fe_{2.11}O_4 + 0.1\ TiO_2$ heat treated at 1250°C in O_2.

For Eq. (1)	cation/anion balance	$\alpha = x(3y/4 - 1)$	(4)
For Eq. (2)	charge balance	$k = x(2y - 8/3)$	(5)
For Eq. (3)	cation/anion balance	$\beta = 4(\alpha + x)/3$	(6)
	charge balance	$\beta = xy - k/2$	(7)
	oxygen balance	$n = (xy - \beta/2 = k/4)$	(8)

All of these quantities in Eq. (3) can therefore be evaluated from the experimental measurements of the weight percent Fe^{2+} in the quenched samples. This mea-

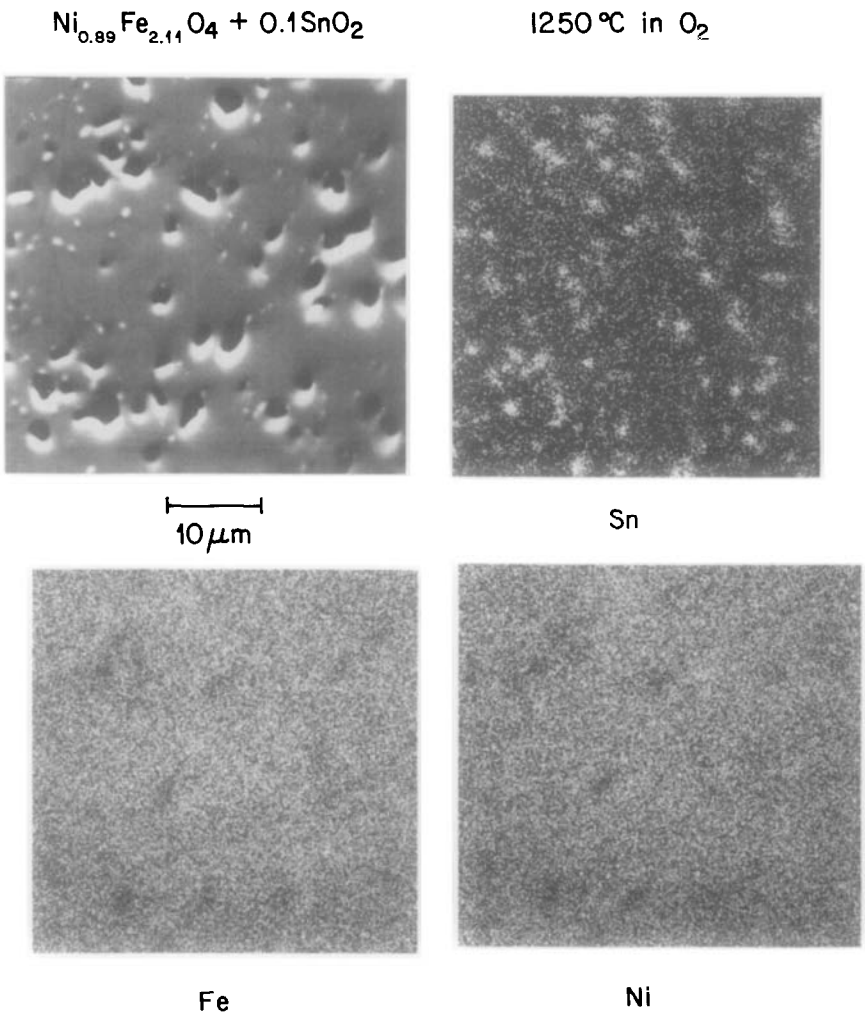

FIG. 3. Electron and elemental characteristic X-ray images of $Ni_{0.89}Fe_{2.11}O_4$ + 0.1 SnO_2 heat treated at 1250°C in O_2.

TABLE IV

MICROPROBE ANALYSIS: TYPE II MATERIALS—SPINEL + HEMATITE/SnO_2 FIRED AT 1250°C IN O_2

Dopant	Phase	Composition	Fe/Ni
0.1 Ti	Spinel	$Ni_{0.925}Fe_{2.075}Ti_{0.066}O_{4+\beta}$	2.24
	Hematite	$Ni_{0.313}Fe_{1.390}Ti_{0.296}O_3$	4.43
0.1 Sn	Spinel	$Ni_{0.924}Fe_{2.076}Sn_{0.036}O_{4+\beta}$	2.25
	SnO_2	Particles too small for analysis—very high in Sn	—
0.1 (Ti + Sn)	Spinel	$Ni_{0.911}Fe_{2.089}Ti_{0.020}Sn_{0.034}O_{4+\beta}$	2.29
	Hematite	$Ni_{0.263}Fe_{1.432}Ti_{0.53}Sn_{0.153}O_3$	5.45

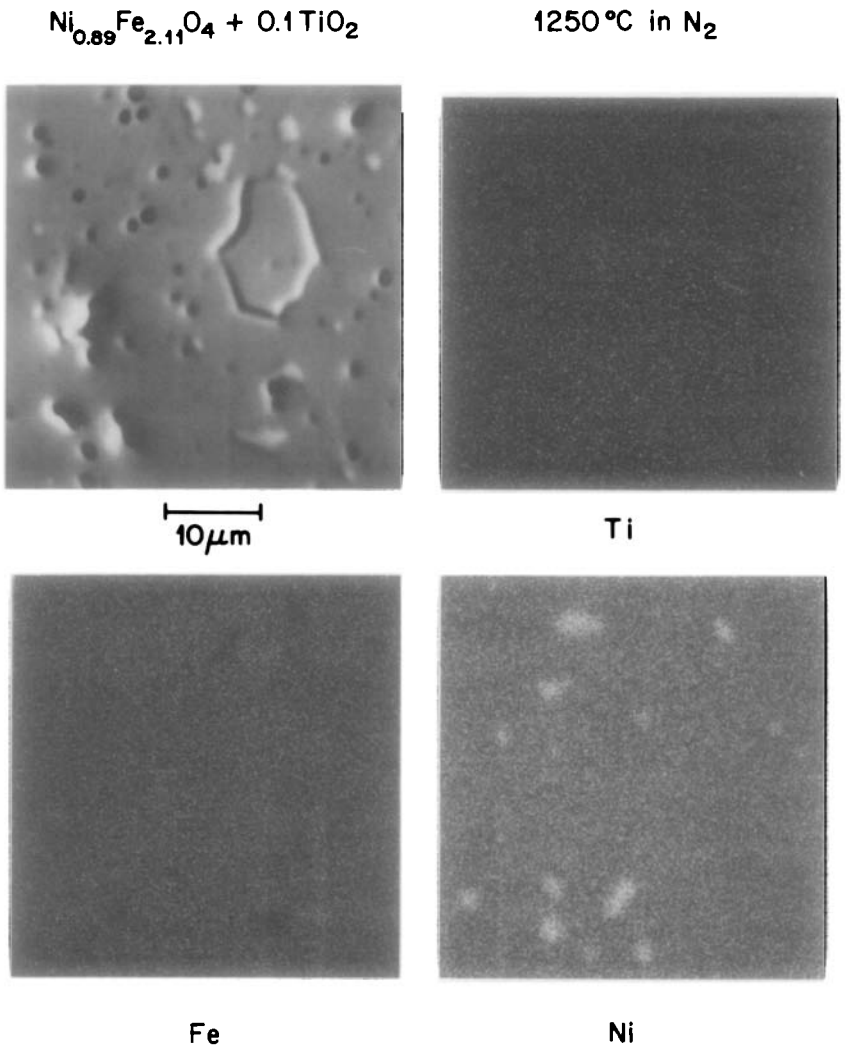

FIG. 4. Electron and elemental characteristic X-ray images of $Ni_{0.89}Fe_{2.11}O_4 + 0.1\ TiO_2$ heat treated at 1250°C in N_2.

sure of total Fe^{2+} allows the calculation of k. When dealing with the single phase spinel region, x and y are known from the nature of the additions and it is then possible to calculate β from Eq. (7). Using these values of β and x in Eq. (6) leads to the associated value of α.

A typical set of experimental data is shown in Fig. 5. The samples at highest Sn and Mg concentrations have a small amount of second phase, SnO_2 and (NiFeMg)O, respectively, present under the firing conditions of 1250°C and 0.1% O_2. Precipitation of a second phase is reflected as a change of slope of such plots in accordance with the accompanying change of excess iron content in the spinel (Fe/Ni ratio), as described in the earlier work (*1*).

The value of α, k, and β derived from data such as in Fig. 5, are plotted in Figs. 6 and 7 for conditions which come the closest to being single phase throughout the range

TABLE V

MICROPROBE ANALYSIS: TYPE III MATERIALS—SPINEL + (NiFe)O FIRED AT 1250°C IN N_2

Dopant	Phase	Composition	Fe/Ni
0.025 Ti	Spinel	$Ni_{0.888}Fe_{2.112}Ti_{0.016}O_{4+\beta}$	2.38
	Monoxide	$Ni_{0.630}Fe_{0.369}Ti_{0.001}O$	0.59
0.025 Sn	Spinel	$Ni_{0.850}Fe_{2.150}Sn_{0.017}O_{4+\beta}$	2.53
	Monoxide	$Ni_{0.614}Fe_{0.386}Sn_{0.000}$	0.63
0.025 (Ti + Sn)	Spinel	$Ni_{0.885}Fe_{2.115}M_{0.014}O_{4+\beta}$	2.39
	Monoxide	$Ni_{0.651}Fe_{0.347}M_{0.002}O$	0.53
0.025 Ga	Spinel	$Ni_{0.883}Fe_{2.117}Ga_{.024}O_{4+\beta}$	2.40
	Monoxide	$Ni_{0.654}Fe_{0.345}G_{.001}O$	0.53
0.1 Mg	Spinel	$Ni_{0.820}Fe_{2.180}Mg_{0.097}O_{4+\beta}$	2.67
	Monoxide	$Ni_{0.558}Fe_{0.281}Mg_{0.131}O$	0.48

of x. The points at highest Sn concentration show the effects of second phase precipitation. The firing conditions are naturally different between Figs. 6 and 7 because the quadrivalent ions require a higher temperature (more reducing conditions) in order to maintain the single phase spinel region over a wide range of x. Tables VII, VIII, and IX summarize the least-squares slopes of the assumed straight lines such as those in Figs. 6 and 7. Slopes are tabulated only for those firing conditions which give rise to a wide range of solubility. There is an inverse relationship between $d\alpha/dx$ and dk/dx that is derived from Eqs. (6) and (7) and which is satisfied in Tables VII–IX.

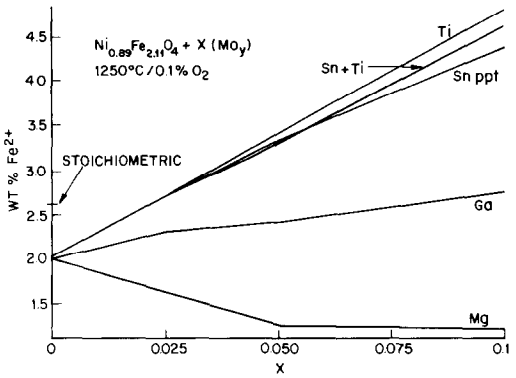

FIG. 5. Weight percent of Fe^{2+} in $Ni_{0.89}Fe_{2.11}O_4$ + xMO_y heat treated at 1250°C in 0.1% O_2.

$$\frac{dk}{dx} = 2y - 8\left(1 + \frac{d\alpha}{dx}\right)\Big/3. \qquad (9)$$

By comparison with the hypothetical values for these slopes in Table VI it is possible to determine the portion of the actual charge compensation that goes by each of these mechanisms and those values are also included in the Tables.

Values of the intercepts at $x = 0$ should be independent of the substitutions and the average values are given in Table X.

The trends obvious in Table X are as anticipated. At constant temperature the vacancy concentration increases and the Fe^{2+} concentration decreases with increasing P_{O_2}. For a constant atmosphere the vacancy content decreases and the Fe^{2+}

TABLE VI

RATE OF CHANGE OF VACANCY CONTENT (α) OR DIVALENT IRON CONTENT (k) AS A FUNCTION OF ADDITIVE CONCENTRATION (x) FOR HYPOTHETICAL CHARGE COMPENSATION MECHANISMS

Valence of additive	$\left(\frac{\partial\alpha}{\partial x}\right)_k^a$	$\left(\frac{\partial\kappa}{\partial x}\right)_\alpha^b$
+4	0.500	1.333
+3	0.125	0.333
+2	−0.250	−0.667

[a] See Eq. (1).
[b] See Eq. (2).

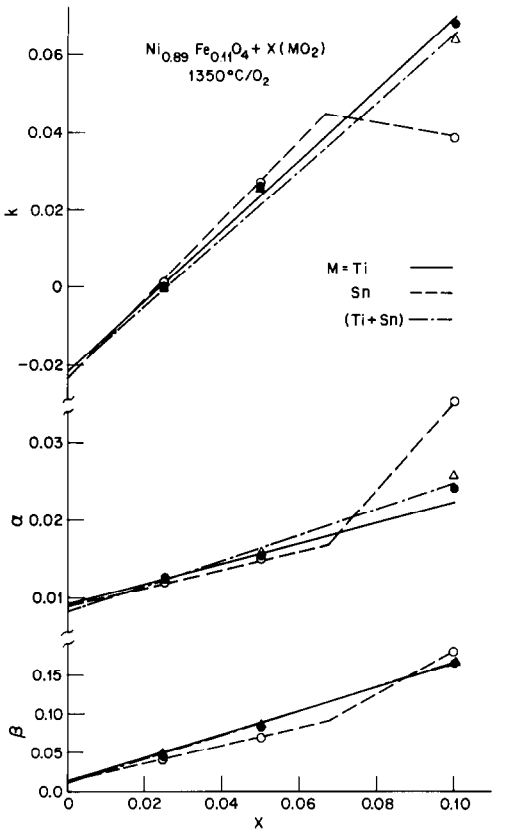

FIG. 6. Values of α, k, and β calculated for $Ni_{0.89}Fe_{2.11}O_4 + xMO_2$ heat treated at 1350°C in O_2.

concentration increases with increasing temperature. Analogous trends can be seen in Tables VII, VIII, and IX. These trends lead to the conclusion that the charge compensation mechanism shifts so that the portion due to vacancy formation increases with decreasing temperature and increasing P_{O_2}. This portion tends to vanish under the reducing conditions and seems to approach about one-third at the most oxidizing conditions.

The replacement of Ti^{4+} by Sn^{4+} does not produce consistent trends with temperature of P_{O_2}. It cannot be established whether this is due to changes in ion size, site distribution, or chemical bonding. Changes in these latter two factors may also affect the earlier comparisons as a function of temperature.

Comparisons of the effects of the charge of the substituted ions indicate virtually no difference under the more oxidizing conditions. Under reducing conditions the Ga^{3+} seems less effective in inducing vacancy formation (Table VIII). Again, this may be related to its site preference or size. Of course, all of these trends with respect to vacancy concentration can be thought in opposite terms in regards to the formation of divalent iron.

In several cases of Type II samples the calculation of α was made as though the sample were single-phase spinel. This value of α coupled with the adjacent value at lower x, where the system was single phase, represents an upper and lower

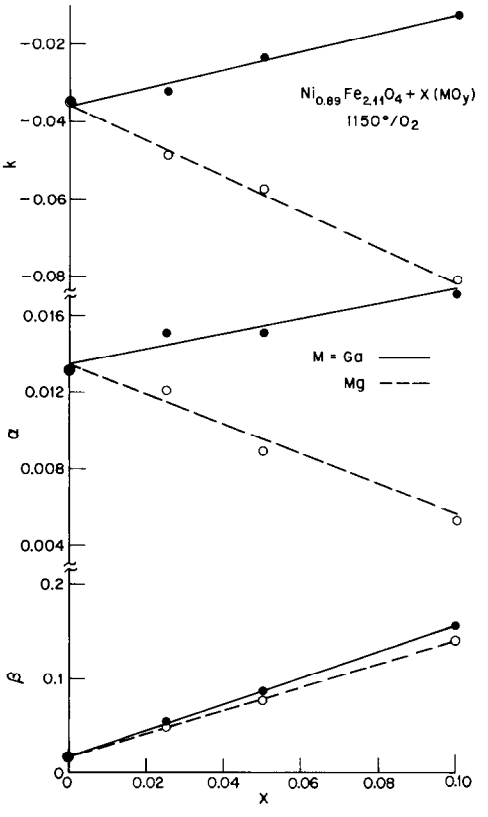

FIG. 7. Values of α, k, and β calculated for $Ni_{0.89}Fe_{2.11}O_4 + xMO_y$ heat treated at 1150°C in O_2.

TABLE VII

EXPERIMENTAL RATES OF CHANGE OF VACANCY (α) AND DIVALENT IRON (k) CONTENTS OF $Ni_{0.89}Fe_{2.11}O_4$ AS A FUNCTION OF TiO_2 OR $(TiSn)O_2$ CONCENTRATION (x) AND PERCENTAGE OF THE CHARGE COMPENSATION VIA EACH MECHANISM FOR SINGLE-PHASE SPINEL[a]

Firing conditions		TiO_2				$(TiSn)O_2$				SnO_2			
(°C)	(% O_2)	$\frac{d\alpha}{dx}$	%	$\frac{dk}{dx}$	%	$\frac{d\alpha}{dx}$	%	$\frac{dk}{dx}$	%	$\frac{d\alpha}{dx}$	%	$\frac{dk}{dx}$	%
1350	0[b]	—	—	—	—	—	—	—	—	—	—	—	—
	0.1[b]	—	—	—	—	—	—	—	—	—	—	—	—
	100	0.154	31	0.921	69	0.169	34	0.879	66	0.122	25	1.004	75
1250	0[b]	—	—	—	—	—	—	—	—	—	—	—	
	0.1[b]	0.045	9	1.215	91	0.065	13	1.162	87	0.092	18	1.088	82
	100[b]	—	—	—	—	—	—	—	—	—	—	—	—
1150	0	0.077	15	1.127	85	0.108	22	1.045	78	0.113	23	1.029	77
	0.1	0.082	16	1.114	84	0.144	29	0.951	71	0.046	9	1.208	91
	100[b]	—	—	—	—	—	—	—	—	—	—	—	—

[a] See Eqs. (1)–(3).
[b] Not single phase over the range in x.

bounds for α_c, the critical value of α at the phase boundary. Figure 8 shows how α_c varies as a function of temperature for several systems. The closed points represent Ni or NiZn ferrites (*9*) while the open points are those for MnZn ferrites (*1*, *10*). The circles are from gravimetric data on undoped ($x = 0$) material. The squares are based upon data where additives are also present. It appears that the specific cause of

TABLE VIII

EXPERIMENTAL RATE OF CHANGE OF VACANCY (α) AND DIVALENT IRON (k) CONTENT OF $Ni_{0.89}Fe_{2.11}O_4$ AS A FUNCTION OF Ga_2O_3 CONCENTRATION (x) AND PERCENTAGE OF THE CHARGE COMPENSATION VIA EACH MECHANISM FOR SINGLE-PHASE SPINEL[a]

Firing conditions					
°C	% O_2	$\frac{d\alpha}{dx}$	%	$\frac{dk}{dx}$	%
1350	0[b]	—	—	—	—
	0.1[b]	—	—	—	—
	100	0.000	0	0.333	100
1250	0[b]	—	—	—	—
	0.1	0.000	0	0.333	100
	100	0.006	5	0.325	95
1150	0[b]	—	—	—	—
	0.1	0.038	30	0.232	70
	100	0.037	30	0.235	70

[a] See Eqs. (1)—(3).
[b] Not single phase over the range of x.

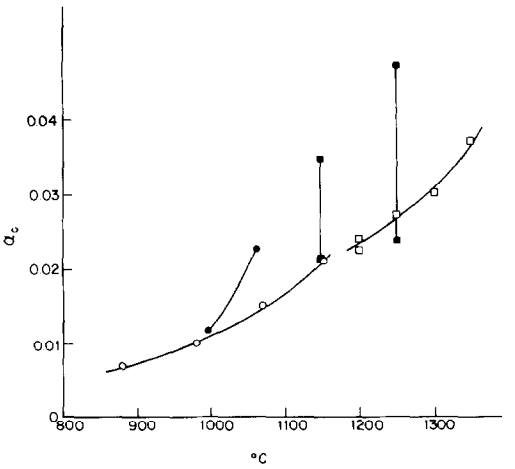

FIG. 8. Values of the vacancy content (α_c) at the spinel/hematite phase boundary. Open points MnZn ferrite (*1*, *10*); close points Ni or NiZn ferrite (*9*); circles gravimetric data x = (*9*, *10*); squares Fe^{2+} analysis ($x \neq 0$).

TABLE IX

EXPERIMENTAL RATE OF CHANGE OF VACANCY (α) AND DIVALENT IRON (k) CONTENTS OF $Ni_{0.89}Fe_{2.11}O_4$ AS A FUNCTION OF MgO CONCENTRATION (x) AND PERCENTAGE OF THE CHARGED COMPENSATION VIA EACH MECHANISM FOR THE SINGLE-PHASE SPINEL

Firing conditions					
°C	$\%O_2$	$\frac{d\alpha}{dx}$	%	$\frac{dk}{dx}$	%
1350	0[b]	—	—	—	—
	0.1[b]	—	—	—	—
	100	−0.075	30	−0.468	70
1250	0[b]	—	—	—	—
	0.1	−0.018	7	−0.620	93
	100	−0.077	31	−0.462	69
1150	0[b]	—	—	—	—
	0.1	−0.039	16	−0.561	84
	100	−0.082	33	−0.452	67

[a] See Eqs. (1)–(3).

[b] Not single phase over the range of x.

the cation vacancies is not particularly important and the doped curve is essentially an extrapolation of the undoped materials. The Ni or NiZn ferrites seem to be somewhat more tolerant of cation vacancies than the MnZn ferrite.

Lattice Parameter of the Spinel Phase

Interpretation of the change in lattice size is complicated by the interplay of the vacancy content, divalent iron concentration, and size and concentration of the additive ion. Only single-phase samples are discussed. Figure 9 shows how the cubic lattice parameter (a) varies with α or k for samples without the complication of any additives. It is unfortunately not possible to vary α and k independently. The lattice should expand as trivalent iron is changed to the larger divalent iron in the absence of other effects. The effect of vacancies should be the opposite allowing for a collapse of the lattice with increasing cation vacancy content regardless of the particular site selection. Both mechanisms predict a lattice shrinkage with oxidation. If one considers the change in lattice parameter going from Fe_3O_4 to γ-Fe_2O_3, the $\Delta a/\Delta\alpha$ is −0.14. The least-squares straight line through four points in Fig. 9 gives a value of −0.14 for $da/d\alpha$ or 0.028 for da/dk.

A similar plot is made for samples having a constant addition of 0.05 Ga_2O_3 in Fig. 10. There is a shift to smaller values of "a"

TABLE X

VALUES OF THE VACANCY CONCENTRATION (α_0), DIVALENT IRON CONTENT (k_0), AND EXCESS OXYGEN (β_0) OF $Ni_{0.89}Fe_{2.11}O_4$ AS A FUNCTION OF FIRING CONDITIONS

Firing conditions		α_0		$-k_0$		β_0	
°C	$\%O_2$	Analyzed[a]	Intercept[b]	Analyzed[a]	Intercept[b]	Analyzed[a]	Intercept[b]
1350	0[c]	—	—	—	—	—	—
	0.1[c]	—	—	—	—	—	—
	100	0.0102	0.0094	0.0273	0.0270	0.0136	0.0132
1250	0[c]	—	—	—	—	—	—
	0.1	0.0096	0.0092	0.0254	0.0246	0.0127	0.0122
	100	0.0118	0.0120	0.0308	0.0330	0.0156	0.0165
1150	0	0.0040	0.0047	0.0106	0.0123	0.0053	0.0067
	0.1	0.0098	0.0098	0.0250	0.0254	0.0130	0.0127
	100	0.0138	0.0135	0.0342	0.0360	0.0171	0.0180

[a] Average of two sets of analyses on separate firings.

[b] Calculated from the average intercept of straight lines from Tables VII, VIII, and IX.

[c] Two phases.

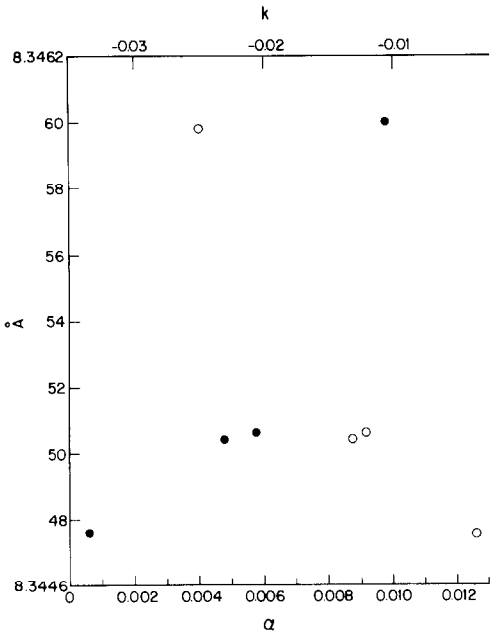

FIG. 9. Variation of the lattice parameter of $Ni_{0.89}Fe_{2.11}O_4$ as a function of α and k. ○, α; ●, k.

because of the substitution of the small Ga^{3+} (0.62 Å) ion into the lattice. The values of $da/d\alpha$ and da/dk are -0.10 and 0.037, respectively. Therefore there are subtle effects due to the substitutions which preclude a constant set of such coefficients to predict changes in the lattice constant upon oxidation/reduction.

A logical factor in the change of lattice parameter is the size of the substituted ion. Values of "a" are selected for samples having nearly identical vacancy concentrations (± 0.0001 in α) but varying x and are plotted in Fig. 11. These values are selected from different temperatures and atmospheres so there may also be variances in the site distribution. At constant α and increasing x the value of k must also be increasing significantly for Ti^{4+} and Ga^{3+} and this would lead to an expansion of the lattice. The opposite would be true for Mg^{2+}. Considering this factor, the very large slope of the Ti^{4+} line is partially due to Fe^{2+} formation. The slope of the Mg^{2+} line would be greater and the Ga^{3+} would be slightly less if not for the Fe^{2+} formation. With these approximate adjustments, the slopes would more closely reflect the difference in the sizes of the three ions.

Conclusions

(1) Additions of TiO_2 and Ga_2O_3 to Ni ferrite, encourage the formation of a hematite phase and tend to concentrate in this oxidized phase. SnO_2 has more limited solubility in the spinel, particularly at high P_{O_2}.

(2) Addition of MgO encourages the precipitation of a monoxide phase in which the Ni and Mg concentrate.

(3) The charge compensation mechanism associated with the solubility of foreign ions into the spinel phase involves changes in both the Fe^{2+} and vacancy concentrations. Under the more oxidizing conditions about $\frac{1}{3}$ proceeds via vacancy formation but this decreases markedly as the conditions become less oxidizing, i.e., higher temperature and lower P_{O_2}.

(4) The vacancy content at the phase

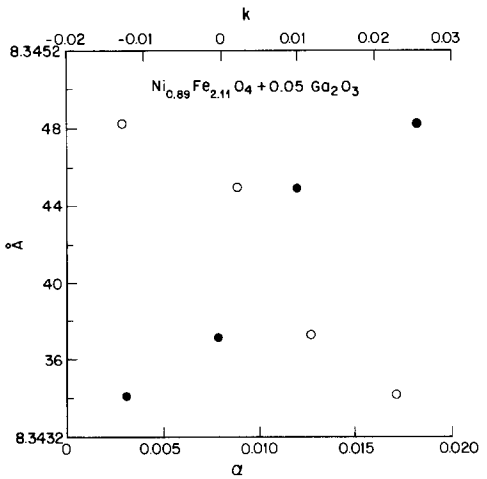

FIG. 10. Variation of the lattice parameter of $Ni_{0.89}Fe_{2.11}O_4 + 0.05\ Ga_2O_3$ as a function of α and k. ○, α; ●, k.

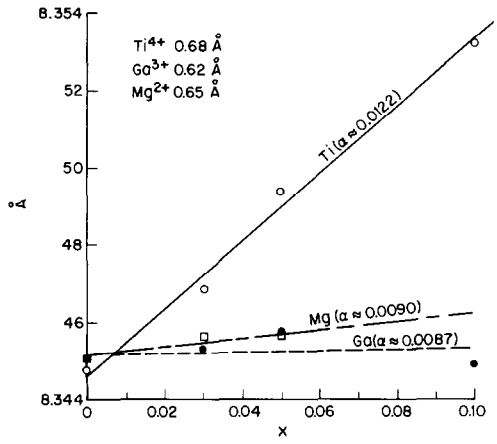

FIG. 11. Variation of the lattice parameter at constant α, of $Ni_{0.89}Fe_{2.11}O_4 + xMO_y$ as a function of x.

boundary associated with hematite precipitation increases with increasing temperature and is somewhat higher than that observed for MnZn ferrite in previous work (*1*) Vacancy content at precipitation appears to be essentially independent of whether the vacancies are induced by substitutions or by firing conditions.

(5) The lattice parameter of the spinel increases with increasing divalent iron content and decreases with increasing cation vacancy content. The rates of these changes are not independent of the amount or nature of cation substitutions. Taking the above factors into consideration the change in lattice parameter at constant vacancy concentration is consistent with the size and amount of cation additions.

(6) The conclusions derived earlier for Ti^{4+} additions to MnZn ferrite (*1*) have been confirmed in this study. Furthermore, it is confidently expected that the extended qualitative relationships listed above for this work on Ni ferrite are also valid for MnZn and other ferrite systems.

Appendix

AVERAGE VALUES OF Wt% Fe^{2+} FOR FIRED AND QUENCHED SAMPLES ($Ni_{0.89}Fe_{2.11}O_4 + xMO_y$)

		1150°C[a]			1250°C[a]			1350°C[a]		
M	*x*	10^{-6}	10^{-3}	10^{0}	10^{-6}	10^{-3}	10^{0}	10^{-6}	10^{-3}	10^{0}
None	0.000	2.37	2.00	1.80	3.84	2.02	1.88	8.11	2.72	1.97
Ti	0.025	2.93	2.73	2.08	3.74	2.72	2.50	7.10	2.88	2.60
Ti	0.500	3.56	3.42	1.81	4.09	3.41	2.86	7.14	3.48	3.19
Ti	0.100	4.98	4.50	1.54	4.80	4.78	2.54	6.67	4.81	4.13
Sn	0.025	2.92	2.58	2.09	3.74	2.71	2.48	6.69	2.85	2.62
Sn	0.050	3.43	3.30	2.05	3.70	3.33	2.44	6.19	3.36	3.17
Sn	0.100	4.55	3.21	2.07	4.50	4.37	2.43	6.08	4.38	3.34
(TiSn)	0.025	2.83	2.67	2.06	3.67	2.71	2.40	6.53	2.90	2.60
(TiSn)	0.050	3.42	3.26	1.89	3.65	3.30	2.69	6.30	3.30	3.18
(TiSn)	0.100	4.62	4.07	1.59	4.37	4.60	2.71	5.94	4.53	3.98
Ga	0.025	2.41	2.14	1.84	3.39	2.32	2.06	6.64	2.78	2.25
Ga	0.050	2.69	2.19	2.02	3.37	2.42	2.24	6.25	2.65	2.43
Ga	0.100	3.17	2.50	2.24	3.15	2.75	2.51	5.81	3.11	2.72
Mg	0.025	2.19	1.66	1.45	3.54	1.61	1.56	7.21	3.03	1.64
Mg	0.050	2.01	1.22	1.25	3.37	1.25	1.24	6.92	3.05	1.31
Mg	0.100	1.75	0.69	0.68	3.44	1.19	0.73	7.13	3.00	0.76

[a] Atmosphere (O_2).

AVERAGE VALUES OF Wt% Fe^{2+} FOR FIRED AND QUENCHED SAMPLES ($Ni_{1.10}Fe_{1.90}O_4 + xMO_y$)

		1150°C[a]			1250°C[a]			1350°C[a]		
M	*x*	10^{-6}	10^{-3}	10^{0}	10^{-6}	10^{-3}	10^{0}	10^{-6}	10^{-3}	10^{0}
None	0.000	1.59	0.37	−0.04	3.82	1.17	0.02	8.72	2.92	0.20
Ti	0.025	1.69	0.39	0.00	3.45	1.31	−0.03	8.29	3.36	0.24
Ti	0.050	1.77	0.42	0.02	3.73	1.38	0.00	8.24	3.45	0.28
Ti	0.100	1.84	0.50	0.28	3.31	1.40	0.28	7.76	3.49	0.40
Sn	0.025	1.53	0.45	0.00	3.13	1.33	0.02	7.35	3.37	0.26
Sn	0.050	1.68	0.52	0.04	3.41	1.33	0.01	7.09	3.40	0.26
Sn	0.100	1.62	0.54	0.25	3.12	1.37	0.50	7.13	3.38	0.58
(TiSn)	0.025	1.51	0.33	0.02	3.28	1.34	0.00	7.12	3.42	0.33
(TiSn)	0.050	1.58	0.54	0.00	3.31	1.38	0.02	6.83	3.38	0.33
(TiSn)	0.100	1.63	0.45	0.41	3.19	1.33	0.46	6.49	3.20	0.37
Ga	0.025	1.56	0.39	−0.07	3.32	1.24	−0.03	7.72	2.92	0.17
Ga	0.050	1.47	0.34	−0.06	3.32	1.23	−0.03	7.00	2.75	0.19
Ga	0.100	1.58	0.49	−0.01	2.96	1.27	0.14	6.17	2.67	0.26
Mg	0.025	1.63	0.45	−0.08	3.72	1.49	0.12	7.92	3.06	0.31
Mg	0.050	1.58	0.43	−0.08	4.00	1.45	0.07	7.93	3.36	0.44
Mg	0.100	1.70	0.47	−0.12	4.17	1.57	0.06	8.71	3.17	0.17

[a] Atmosphere (O_2).

Acknowledgment

The authors are grateful to Mr. F. Schrey for chemical analysis of the starting compositions.

References

1. D. W. JOHNSON, JR., P. K. GALLAGHER, M. F. YAN, AND H. SCHREIBER, *J. Solid State Chem.* **30**, 299–310.
2. R. MORINEAU, *Phys. Stat. Sol. A* **38**, 559 (1976).
3. P. K. GALLAGHER, E. M. GYORGY, AND D. W. JOHNSON, *Amer. Cer. Soc. Bull.* **57**, 812 (1978).
4. H. M. O'BRYAN, F. R. MONFORTE, AND R. BLAIR, *J. Amer. Cer. Soc.* **48**, 577 (1965).
5. I. HANKE AND M. ZENGER, *J. Mag. Magn. Materials* **4**, 120 (1977).
6. D. W. JOHNSON AND P. K. GALLAGHER, *in* "Ceramic Processing Before Firing" (G. Y. Onada and L. L. Hench, Eds.), p. 125. Wiley, New York (1978).
7. P. K. GALLAGHER, *Amer. Cer. Soc. Bull.* **57**, 576 (1978).
8. J. W. COLBY, "Proc. Sixth Nat. Conf. on Electron Probe Analysis," 1971, paper #17, Electron Prob. Anal. Soc.
9. P. BRACCONI AND P. K. GALLAGHER, *J. Amer. Cer. Soc.* **62**, 172 (1979).
10. P. I. SLICK, *in* "Ferrites: Proc. Int. Conf., July 1970" (Y. Hashino, S. Iida, and M. Sugimoto, Eds.), p. 191. Univ. of Tokyo Press, Tokyo, Japan (1971).